Identification of the Binding Region of the [2Fe-2S] Ferredoxin in Stearoyl-Acyl Carrier Protein Desaturase: Insight into the Catalytic Complex and Mechanism of Action†

Pablo Sobrado,‡ Karen S. Lyle,‡ Steven P. Kaul, Michelle M. Turco, Ida Arabshahi, Ashok Marwah, and Brian G. Fox*

Department of Biochemistry, College of Agricultural and Life Sciences, University of Wisconsin, Madison, Wisconsin 53706

Received January 10, 2006; Revised Manuscript Received February 20, 2006

ABSTRACT: Stearoyl-acyl carrier protein desaturase (Δ9D) catalyzes the O_2 and $2e^-$ dependent desaturation of stearoyl-acyl carrier protein (18:0-ACP) to yield oleoyl-ACP (18:1-ACP). The $2e^-$ are provided by essential interactions with reduced plant-type [2Fe-2S] ferredoxin (Fd). We have investigated the protein−protein interface involved in the Fd−Δ9D complex by the use of chemical cross-linking, site-directed mutagenesis, steady-state kinetic approaches, and molecular docking studies. The treatment of the different proteins with 1-ethyl-3-(3-dimethylaminopropyl)carbodiimide and *N*-hydroxysuccinimide revealed that carboxylate residues from Fd and lysine residues from Δ9D contribute to cross-linking. The single substitutions of K60A, K56A, and K230A on Δ9D decreased the k_{cat}/K_M for Fd by 4-, 22-, and 2400-fold, respectively, as compared to wt Δ9D and a K41A substitution. The double substitution K56A/K60A decreased the k_{cat}/K_M for Fd by 250-fold, whereas the triple mutation K56A/K60A/K230A decreased the k_{cat}/K_M for Fd by at least 700 000-fold. These results strongly implicate the triad of K56, K60, and K230 of Δ9D in the formation of a catalytic complex with Fd. Molecular docking studies indicate that electrostatic interactions between K56 and K60 and the carboxylate groups on Fd may situate the [2Fe-2S] cluster of Fd closer to W62, a surface residue that is structurally conserved in both ribonucleotide reductase and mycobacterial putative acyl-ACP desaturase DesA2. Owing to the considerably larger effects on catalysis, K230 appears to have other contributions to catalysis arising from its positioning in helix 7 and its close spatial location to the diiron center ligands E229 and H232. These results are considered in the light of the presently available models for Fd-mediated electron transfer in Δ9D and other protein−protein complexes.

Stearoyl-acyl carrier protein Δ^9 desaturase (Δ9D)[1] catalyzes the O_2- and NAD(P)H-dependent insertions of a cis double bond between carbons 9 and 10 of 18:0-ACP to yield 18:1-ACP. This soluble, homodimeric enzyme (M_r 84 000) contains a catalytically essential diiron cofactor in each subunit. The diiron center is maintained in the active site by endogenous ligands derived from two copies of the sequence motif (D/E)-$X_{\sim 40}EX_2H$ separated by ∼100 amino acids (*1*). Related diiron binding motifs are found in other desaturases (*2*), the R2 component of ribonucleotide diphosphate reductase (*3*), and the bacterial hydrocarbon hydroxylases (*4*). The catalytic cycle for these enzymes consists of substrate binding, electron transfer to form a diferrous center, and O_2 activation as essential prerequisites to substrate oxidation (*5*−*7*). In addition, ferritin (*8*) and rubrerythrin (*9*) have related diiron centers but differ in their catalytic cycles.

An acyl-ACP and a reduced plant-type [2Fe-2S] ferredoxin are both required for efficient Δ9D catalysis (*10*). ACP, a small, negatively charged protein, enhances the K_M value for the 18-carbon acyl chain relative to the comparable acyl-CoA (*11*), whereas k_{cat} and k_{cat}/K_M values are enhanced by hydrophobic contributions from the acyl chain (*10*). The addition of stoichiometric 18:0-ACP to sodium dithionite-reduced Δ9D ($4e^-$ Δ9D) changed the coordination geometry and the redox-active orbitals of the diiron center (*12*) such that the reactivity with O_2 might be enhanced (*13*), and indeed, the addition of O_2 to the complex of 18:0-ACP and $4e^-$ Δ9D yielded a quasi-stable μ-1,2 peroxo species (*14*, *15*). However, this peroxo species ultimately decayed without the formation of 18:1-ACP and without the release of H_2O_2 (*14*), suggesting that key elements contributing to catalysis were missing from the simplified reaction system.

In contrast to the results described above with chemically reduced Δ9D, Fd is a catalytically competent electron donor

† This work was supported by the National Institutes of Health Grant GM-50853 to B.G.F. P.S. was supported in part by a postdoctoral fellowship from CONICIT-Costa Rica (Grant 295-2004). K.S.L. was a trainee of the NIH Institutional Molecular Biophysics Pre-Doctoral Training Grant T32 GM-08293.

* To whom correspondence should be addressed. Tel: (608) 262-9708. Fax: (608) 265-2904. E-mail: bgfox@biochem.wisc.edu.

‡ These two authors made equal contributions to the completion of this work.

[1] Abbreviations: ACP, acyl carrier protein; 18:0-ACP, ACP with stearic acid covalently attached to ACP through a phosphopantetheine thioester bond; 18:1-ACP, ACP with oleic acid covalently attached to ACP through a phosphopantetheine thioester bond; Δ9D, 18:0-ACP Δ^9 desaturase; resting Δ9D, an isolated form of Δ9D containing all ferric sites; $4e^-$ Δ9D, chemically reduced form of Δ9D containing all ferrous sites; Fd, *Anabaena* 7120 vegetative [2Fe-2S] ferredoxin; GC, gas chromatography; MS, mass spectrometry; EDC, 1-ethyl-3-(3-dimethylaminopropyl)carbodiimide; NHS, *N*-hydroxysuccinimide; BME, β-mercaptoethanol.

10.1021/bi0600547 CCC: $33.50
Published on Web 03/28/2006

for Δ9D during the conversion of 18:0-ACP to 18:1-ACP (*16*). For example, a rapid mix of the Fd-reduced enzyme−substrate complex with an aerobic buffer resulted in a burst phase (k_{burst} = 95 s^{-1}) of product formation accounting for ~90% of the turnover expected from one subunit in the dimeric protein. This rapid phase was followed by a slower phase (k_{linear} = 4.0 s^{-1}) of product formation corresponding to the turnover expected from the second subunit. The reaction of the oxidized enzyme−substrate complex with excess reduced Fd resulted in a slower, linear rate (k_{obs} = 3.4 s^{-1}) of product formation over ~1.5 turnovers/Δ9D active site, implicating the Fd−Δ9D complex formation as a distinct step in the single turnover reaction. However, because the steady-state catalysis has a k_{cat} value ≈0.5 s^{-1}, product release appears to be the rate-limiting step in catalysis.

The significant role for Fd in catalytic desaturation was unexpected because dithionite-reduced preparations of methane monooxygenase (*17*−*20*) and ribonucleotide reductase (*21*) were competent for methane oxidation and tyrosyl radical formation, respectively. Thus, unlike other enzymes in the diiron-enzyme superfamily, Δ9D apparently requires an electron transfer from the biological electron donor, and this requirement may be further mediated by interactions with acyl-ACP.

This work examines potential sites of interaction between Fd and Δ9D by using chemical cross-linking and steady-state kinetic analysis. Figure 1 shows the spatial relationship of the lysine residues investigated in this work in the 3D structure of Δ9D. The results implicate the participation of carboxylate residues from Fd and a triad of lysine residues on the surface of Δ9D in the formation of the catalytic complex. Two of these lysine residues, K56 and K60, cluster close to W62, a surface tryptophan residue that has structurally conserved homologues in ribonucleotide reductase (*22*) and putative acyl-ACP desaturase DesA2 from *Mycobacterium tuberculosis* (*23*). The third, K230, is hydrogen bonded to E233 along a conserved helix opposite to the diiron ligands E229 and H232. Mutagenesis of these three lysine residues to alanine essentially eliminates the ability of Δ9D to recognize Fd as an electron donor. In the discussion section, we consider how protein−protein interactions involving these residues might contribute to Δ9D catalysis.

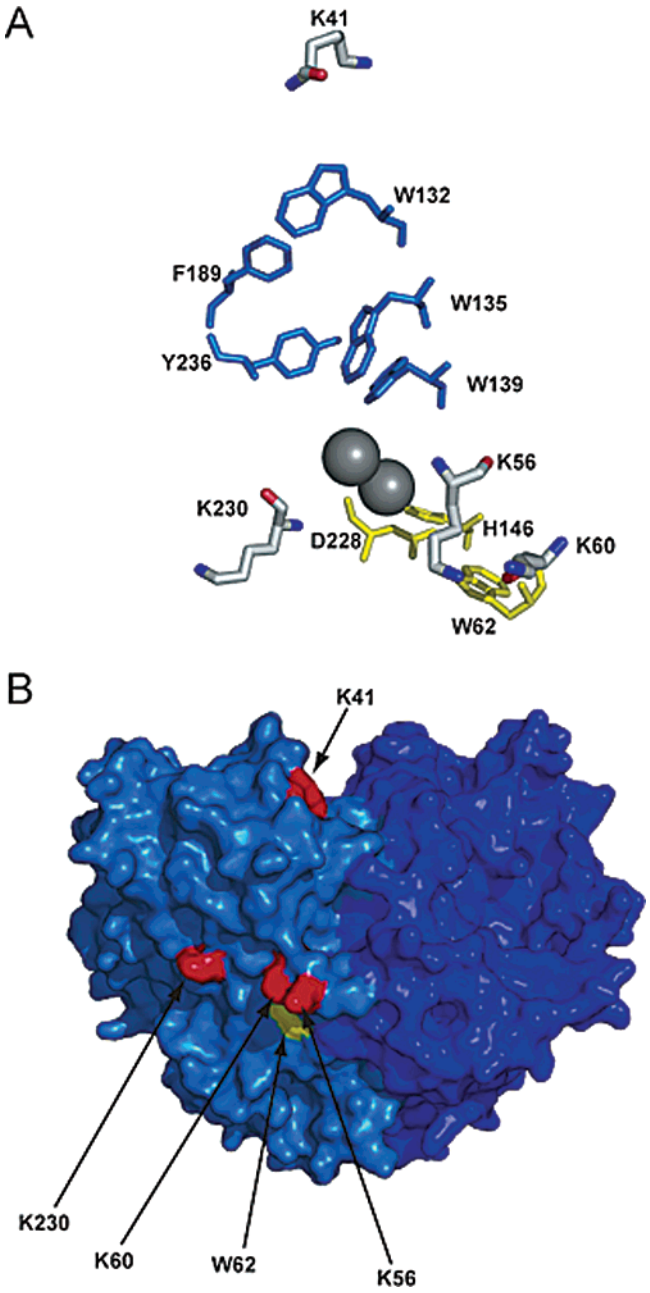

FIGURE 1: (A) Amino acids involved in putative electron-transfer pathways to the diiron center (gray spheres) of Δ9D. One proposed pathway, consisting of W62, D228, and H146 (yellow), extends from the surface of Δ9D and is close to K56, K60, and K230. The other proposed electron-transfer pathway consists of W132, F189, Y236, W135, and W139 (blue) and is closest to K41. (B) Surface representation of the Δ9D dimer showing the relative location of the targeted surface lysines (red) in relation to W62 (yellow). The two subunits of Δ9D are shown in different shades of blue.

MATERIALS AND METHODS

Enzymes. Fd was expressed, purified, and characterized as previously described (*24*). The concentration of Δ9D active sites was determined using ϵ_{340} = 4200 M^{-1} cm^{-1} per diiron center, and cross-correlated by the determination of protein concentration and total iron concentration (*1*). For the preparations of Δ9D and each of the mutated isoforms of Δ9D studied in this work, these quantifications indicate greater than 95% occupation of the diiron active sites in the dimeric protein. Furthermore, the specific activity of the wt Δ9D preparations used in this work matched the range observed in other preparations of the enzyme (*10*). Recombinant *Escherichia coli* and spinach ACP were expressed, purified, phosphopantetheinylated, and acylated as previously described (*10*, *14*). The acyl chains were reductively cleaved, extracted, derivatized, and analyzed by GC-MS as previously described (*10*).

Chemicals. 1-Ethyl-3-(3-dimethylaminopropyl)carbodiimide (EDC) was from Pierce (Rockford, IL). *N*-Hydroxysuccinimide and buffers were from Sigma (Saint Louis, MO). HPLC-grade acetic acid was from Fisher Scientific (Pittsburgh, PA). Methanol and acetonitrile (HPLC-grade) were from Aldrich.

Cross-Linking Reactions. Δ9D and Fd were cross-linked in 25 mM HEPES at pH 7.4, containing 17 mM NaCl using a procedure based upon that of Sehgal et al. (*25*). Δ9D was added to a final concentration of 12.5 μM, Fd was added to a final concentration of 50 μM, and 18:0-ACP was added to a final concentration of 25 μM. The final reaction volume was 50 μL. A stock solution of EDC (50 mM in 25 mM

HEPES at pH 7.4) was prepared ~5 min prior to use and was added to a final concentration of 5 mM to a buffer solution containing either Fd or Δ9D. A stock solution of NHS (50 mM in 25 mM HEPES at pH 7.4) was then added to the EDC-treated protein to a final concentration of 10 mM. This reaction was incubated at room temperature for 5 min, and BME (1.4 M in H_2O) was added to a final concentration of 20 mM and the protein solution incubated again at room temperature. After 5 min, Fd, Δ9D, or premixed Δ9D−18:0-ACP was added to the reaction, and the reaction mixture was incubated for 2 h at 25 °C with shaking. After this incubation period, hydroxylamine (100 or 300 mM in H_2O) was added to the cross-linking reaction to a final concentration of 10 mM. Approximately 15−20 μL of the cross-linking reaction was diluted into a 2X SDS sample buffer and analyzed by SDS−PAGE using BioRAD Tris-HCl Ready-Gels, Criterion gels (BioRad, Hercules, CA), or 10% Tris-tricine gels. The SDS−PAGE gels were stained with Coomassie Brilliant Blue and destained in 10% acetic acid/30% methanol.

Site-Directed Mutagenesis. All of the Δ9D variants carrying the different lysine to alanine single or multiple substitutions were prepared according to the QuikChange protocol (Stratagene, La Jolla, CA). The K41A mutation was generated with the primer 5′-ccccaaaagattgagatctttGCAtc-cctagacaattgggc −3′ and its reverse complement. (The mutated codon is indicated in capital letters.) The K56A mutation was generated with the primer 5′-gaacattctggt-tcatctGGCgccagttgagaaatgttggcaaccgc-3′ and its reverse complement. The K60A mutation was generated with the primer 5′- ctgaagccagttgagGCAtgttggcaaccgc-3′ and its reverse complement, and the double mutation, K56A/K60A, was prepared from the K60A background with the primer 5′-ctggttcatctGGCgccagttgagGCA-3′ and its reverse complement. The K230A mutation was constructed with the primer 5′-gtacaattgctgcagatgagAAGcgccatgagacagcctac-3′ and its reverse complement. The triple mutation, K56A/K60A/K230A, was generated using the same primer as that used for K230A with the gene containing the K56A/K60A mutations as the template. The transformed clones were selected and sequenced by Big Dye DNA sequencing at the University of Wisconsin Biotechnology Center to identify individual clones containing the correct gene sequence.

Protein Expression. For protein expression, 1 μL of plasmid DNA (~0.2 μg) was transformed into *E. coli* BL21-(DE3) cells by electroporation and plated onto Luria−Bertani plates containing 50 μg mL^{-1} kanamycin. Kanamycin-resistant transformants (~3 colonies) were used to inoculate 5 mL of the Luria−Bertani medium containing 50 μg mL^{-1} of kanamycin and 1% (w/v) glucose. This culture was grown at 37 °C with shaking (250 rpm). After the 5-mL culture reached an OD_{600} value of ~0.2, 1 mL of the culture was used to inoculate 50 mL of Luria−Bertani medium containing 50 μg mL^{-1} of kanamycin and 1% (w/v) glucose, and the culture was incubated at 37 °C. After ~4 h, this culture reached an OD_{600} value of ~0.5, and 1 mL of that was used to inoculate each of six 2-L flasks containing 500 mL of Luria−Bertani medium supplemented with 50 μg mL^{-1} of kanamyacin and 1% (w/v) glucose. These cultures were incubated at 37 °C, with shaking at 250 rpm for ~4 h or until they reached an OD_{600} value of ~0.5. The incubation temperature was reduced to 25 °C, and the cultures were induced by the addition of isopropyl-β-D-thiogalactopyranoside to a final concentration of 1 mM. At induction, each 500-mL culture was supplemented with 1 mL of 40 mM $FeSO_4$ and 1 g of Casamino acids. After ~12 h, the cells were harvested by centrifugation for 15 min at 4400*g*. The cell pellets were washed with 50 mM phosphate at pH 7.0, pelleted by centrifugation for 15 min at 39 000*g*, and stored at −80 °C. The growth procedure yielded ~1.0 g L^{-1} of wet cell paste.

Protein Purification. The Δ9D variants bearing the different Lys mutations were purified from *E. coli* using a procedure similar to that previously described (*26*). Approximately 3 g of frozen cell paste was thawed in a small steel beaker (~10 mL) and resuspended in 25 mM HEPES at pH 8.0. The cells were incubated on ice for 10 min after the addition of 25 mg each of lysozyme, RNase, and DNase to the cell suspension. The cell mixture was sonicated for a total of 1 min using 10-s pulses (Fisher Model 550 Sonic Dismembrator, 1/8-in horn, and 45% maximum output). During sonication, the temperature of the cell suspension was maintained below 10 °C by placing the beaker in an ice-water bath containing NaCl. The suspension was diluted to 50 mL in 25 mM HEPES at pH 8.0 and centrifuged for 1 h at 39 000*g* to remove cell debris. The supernatant was loaded onto a 30 mL Q-Sepharose column equilibrated in 25 mM HEPES at pH 8.0. The column was washed with 50 mL of 25 mM HEPES at pH 8.0, and the protein was eluted in a 0.2-L linear gradient from 0 to 0.23 M NaCl in 25 mM HEPES at pH 8.0, at a linear flow rate of 7.6 cm h^{-1}. Fractions were analyzed by SDS−PAGE, and fractions containing Δ9D were pooled and concentrated by ultrafiltration (YM30 membrane, Amicon Inc., Beverly, MA). The concentrated sample was loaded onto a HiPrep 26/60 Sepharacyl S-100 column (Pharmacia LKB Biotechnology Inc., Piscataway, NJ) equilibrated with 25 mM HEPES at pH 7.8, containing 50 mM NaCl, and eluted at 6.8 cm h^{-1}. Fractions containing Δ9D were identified by SDS−PAGE, pooled, and concentrated by ultrafiltration. Small aliquots of purified protein were frozen in liquid nitrogen and stored at −80 °C.

Steady-State Evaluation of 18:1-ACP Formation. Enzyme reactions were performed in 25 mM HEPES buffer at pH 7.4, containing 17 mM NaCl. Assays contained varying concentrations of Fd, 40 μM *E. coli* or spinach 18:0-ACP, 1.5 μM ferredoxin reductase, and 0.02 or 0.04 nmol of Δ9D in a total volume of 500 μL. The reaction was initiated by the addition of NADPH to a final concentration of 400 μM. Aliquots were removed at timed intervals and quenched by rapid mixing with 200 μL of THF. The initial reaction velocities were determined using linear least-squares fitting from the time-dependence for appearance of the 18:1 products in reactions as determined by GC/EI-MS. The steady-state parameters, k_{cat} and K_M, were determined by nonlinear least-squares fitting of the initial desaturation velocity and substrate concentration data to the Michaelis−Menten equation

$$v = k_{cat}[S]/(K_M + [S]) \quad (1)$$

using Kaleidagraph (Abelbeck Software, Reading, PA).

Mass Spectrometry. Cross-linking reactions were dialyzed in 1 L of 10 mM ammonium acetate at pH 5.0 for ~16 h.

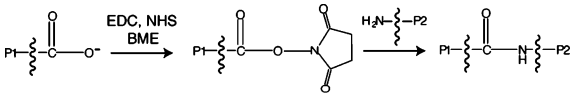

FIGURE 2: Summary of the sequence of reactions used for EDC-catalyzed cross-linking. The carboxylate groups from one protein (P1) are activated with EDC and then reacted with NHS to yield a relatively stable succinimide-ester. The NHS-activated carboxylate group on P1 then reacts with an amine group from protein P2 to generate a new peptide bond between proteins P1 and P2 upon displacement of the succinimide group.

The MALDI-MS analyses were obtained from either an α-cyano or a sinapinic acid matrix using a Bruker BIFLEX III spectrometer equipped with a 337 nm nitrogen laser.

Δ9D-Fd Docking Model. The protein−protein docking web server ClusPro (http://nrc.bu.edu/cluster/) was used to obtain 3D models of the Fd- and ACP- complexes with Δ9D (*27*, *28*). This server provides algorithms that filter docked conformations on the basis of shape complementarity, desolvation, and electrostatic energies. The PDB file 1AFR containing the coordinates for Δ9D was used as the static receptor molecule, and the files, 1FXA, containing the coordinates for [2Fe-2S] ferredoxin (*29*) and the coordinates for ACP[2] were separately used as the moving ligand molecules. The top 60 docked conformations of Fd binding and the top 20 docked conformations of ACP from ZDOCK evaluations were examined in detail.

RESULTS

Covalent Cross-Linking of Fd and Δ9D. The combination of the zero-length cross-linker EDC and NHS can be used to define the source of the carboxyl and amine groups contributing to the cross-link (*25*). Figure 2 shows the reaction mechanism and the sequence of additions used to perform the cross-linking of Fd and Δ9D. In the first step of this sequence, the carboxylate groups on protein P1 were reacted with EDC to form a reactive *O*-acylurea intermediate. By the immediate reaction of the unstable *O*-acylurea intermediate with NHS, a more stable *N*-hydroxysuccinimido ester derivative was formed from the activated carboxyl groups. After the quenching of excess EDC by the addition of BME, the cross-linking reaction was initiated by the addition of protein P2. The amide linkages were formed by the displacement of NHS from P1 by an amine group from P2.

Figure 3 shows the results from several control reactions that were performed to establish the behavior of the individual proteins in the presence of the cross-linking reagents. Lanes 2, 4, and 7 show the products of reactions containing untreated Fd (lane 2), Fd treated with BME-quenched EDC (lane 4), and EDC-activated Fd (lane 7). The products of these reactions were comparable on the basis of the SDS−PAGE analysis. Specifically, Fd appeared as an approximately equal distribution of two bands with apparent masses of ∼10 and ∼22 kDa after treatment with BME at 25 °C for 5 min. Further studies (not shown) revealed that the larger band was the exclusive product obtained from the more vigorous treatment of Fd with BME at 90 °C. The small change in the electrophoretic mobility of the 10-kDa Fd band

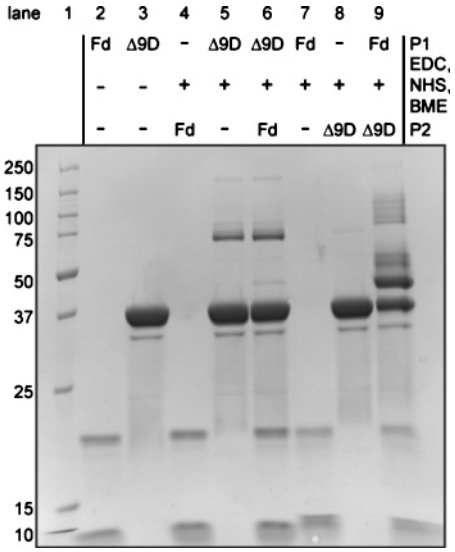

FIGURE 3: Coomassie-stained denaturing electrophoresis gel containing proteins obtained from the indicated cross-linking reactions. The identities of P1 and P2, as defined in Figure 2, are indicated. Lane 1 contains molecular mass standards.

in lanes 7 and 9 may be due to the modifications of the carboxylic groups by EDC and NHS during the P1 reaction. Lanes 3 and 8 in Figure 3 show that the reactions containing untreated Δ9D (lane 3) and Δ9D treated with BME-quenched EDC (lane 8) were also indistinguishable on the basis of the SDS−PAGE analysis. The single band with an apparent mass of 37 kDa apparently corresponded to the Δ9D subunit (M_r 42 000) obtained from denaturation of the dimeric Δ9D by SDS. In contrast, the SDS−PAGE analysis of EDC-activated Δ9D (lane 5) revealed two bands with apparent masses of ∼37 and ∼75 kDa. The ∼37 kDa product corresponded to a single Δ9D subunit (M_r 42 000), whereas the ∼75 kDa band corresponded to a covalent cross-linking of two Δ9D subunits (M_r 84 000). Two possible intersubunit salt bridges in Δ9D that might be activated for amide-bond formation by the EDC and NHS treatment are K152 with E166 and K167 with E59 (i.e., less than 5 Å separation between Lys-NZ and Glu-CD). In addition, there are five possible intrasubunit salt bridges between the lysine and glutamate residues (E38 and K41; E85 and K88; E182 and K261; E233 and K230; and E245 and K242) and three possible intrasubunit salt bridges between lysine and aspartate residues (i.e., less than 5 Å separation between Lys-NZ and Asp-CG; D247 and K36; D257 and K261; and D311 and K312).

Two reaction sequences were used to study the formation of a cross-linked Fd−Δ9D complex. In one reaction sequence, the carboxylate groups from Δ9D were first activated by treatment with EDC and NHS, the excess EDC was quenched by the addition of BME, and then Fd was added. An SDS−PAGE analysis of this reaction sequence (lane 6 in Figure 3) revealed two bands with apparent masses of ∼37 and ∼75 kDa, which is the same result obtained from the reaction of Δ9D alone (lane 5 in Figure 3). In the other reaction sequence, the carboxylate groups from Fd were first activated by treatment with EDC and NHS, the excess EDC was quenched, and then Δ9D was added. An SDS−PAGE analysis of this reaction sequence (lane 9 in Figure 3) revealed two prominent bands with apparent masses of ∼37 and ∼45 kDa and a mixture of other minor, higher-mass

[2] Zornetzer, G. A., Fox, B. G., and Markley, J. L. *Biochemistry*, in press and pdb file 2AVA.

Table 1: MALDI-MS Analysis of Cross-Linked Products Obtained from the Interactions of Fd and Δ9D

species[a]	estimated mass (kDa)[b]	observed peak *m/z* ratios[c]	charge state[d]	calculated *m/z* ratios[e]
Fd	10	10875	$[M + H]^{1+}$	10699
Δ9D	37	41369	$[M + H]^{1+}$	41646
Δ9D		20877	$[M + 2H]^{2+}$	20823
Δ9D−Fd	45	52219	$[M + H]^{1+}$	52345
Δ9D−Fd		26062	$[M + 2H]^{2+}$	26173
Δ9D−Fd−Fd	58	62325	$[M + H]^{1+}$	63044
Δ9D−Δ9D	75	83338	$[M + H]^{1+}$	83292

[a] Fd, [2Fe-2S ferredoxin]; Δ9D, refers to a single subunit of the Δ9D dimer. [b] As determined from SDS−PAGE analysis. [c] Observed mass peak from MALDI-MS analysis performed as described in Materials and Methods. [d] Assigned charge state. [e] Calculated *m/z* from the observed mass peak and assigned charge state.

products. Although the ~37 kDa band represents the unreacted Δ9D subunit, the ~45 kDa product was not observed from any of the other control reactions (lanes 2, 3, 5, 6, and 8 in Figure 3) and roughly corresponded to the combined mass of one Δ9D subunit (~42 kDa) and one Fd (~11 kDa). Thus only the activation of the carboxylate residues on Fd led to cross-linking with Δ9D. It is also noted that the activation of Fd bypassed the formation of the ~75 kDa product assigned to a covalent linkage of the EDC-activated subunits of dimeric Δ9D.

MALDI-MS analyses were performed to more precisely determine the molecular masses of the polypeptides observed by SDS−PAGE. Table 1 shows the assignments made for the three prominent peaks of 10875, 41369, and 52219 *m/z* observed in the MALDI-MS spectrum. These masses closely corresponded to those expected for the singly protonated $[M + H]^+$ Fd (*m/z* 10699), the Δ9D subunit (*m/z* 41646), and the cross-linking of Fd with the Δ9D subunit (*m/z* 52345). Several minor peaks were also observed, which likely represented the $[M + 2H]^{2+}$ ions of the Δ9D subunit (*m/z* 20823), the cross-linked complex of Δ9D and Fd (*m/z* 26173), and the $[M + H]^{1+}$ ion from a single Δ9D subunit cross-linked to 2 Fd (*m/z* 63044).

Mutagenesis of Δ9D and Kinetic Analysis. The results of Figure 3 and Table 1 demonstrated that amide linkages could be formed between Fd and Δ9D but only in reactions where EDC was used to activate the carboxylate groups from Fd. Thus, Δ9D must provide lysine residues to the amide bond-(s) formed in the cross-linking reactions. Figure 1B shows that K41, K56, K60, and K230 are positioned in close proximity to the aromatic amino acids previously identified as possible electron-transfer pathways for Δ9D (*30*) and other members of the diiron superfamily (*22*, *23*).

To examine the potential role of these residues in the formation of an Fd−Δ9D complex, they were mutated to alanine. The mutated Δ9D variants (along with wt Δ9D) were then characterized using steady-state kinetics by varying the concentration of Fd at fixed, saturating concentrations of 18:0-ACP. Figure 4 shows representative v versus [S] plots obtained from these characterizations, whereas Table 2 shows the kinetic parameters obtained from the nonlinear least-squares fitting of the experimental results using eq 1. For wt Δ9D and the K41A mutation, both the k_{cat} value for the formation of 18:1-ACP and the K_M value for Fd were comparable to the kinetic parameters previously determined for wt Δ9D (*10*).

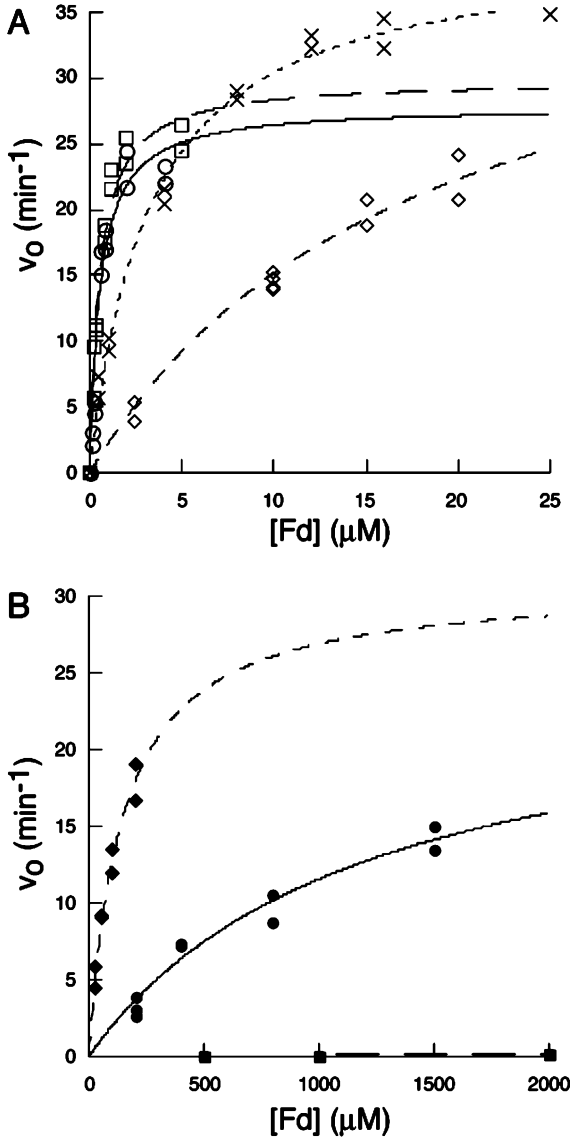

FIGURE 4: Dependence of v_o for 18:1-ACP formation on the concentration of Fd. (A) wt Δ9D, (○); K41A Δ9D, (□); K60A Δ9D, (×); and K56A Δ9D, (◇). (B) K56A/K60A Δ9D, (◆); K230A Δ9D, (●); and K56A/K60A/K230A Δ9D (■). The lines are the results of nonlinear least-squares fitting of the experimental data using eq 1.

The steady-state kinetic analysis revealed that the K56A and K60A variants had k_{cat} values equivalent to wt Δ9D and K41A Δ9D; however, the K_M values determined for these two variants were altered slightly to values ~30-fold and ~6-fold greater, respectively, than the K_M-value determined for wt Δ9D. On the basis of these relatively modest changes in K_M values, the doubly mutated K56A/K60A Δ9D was also generated, and it yielded a k_{cat} value of ~30 min^{-1} (again similar to that for wt Δ9D) along with a K_M value of ~140 μM (an ~250-fold increase in K_M as compared to that for wt Δ9D). Surprisingly, when K230A Δ9D was examined, a K_M value of ~1200 μM was obtained, representing an ~2200-fold decrease in the apparent affinity for Fd. However, the K230A Δ9D also had a k_{cat} value of ~25 min^{-1}, which was only slightly diminished relative to that for wt Δ9D.

To further probe the role of these lysines in Fd binding to Δ9D, the triply mutated K56A/K60A/K230A Δ9D was

Table 2: Kinetic Parameters for the Δ9D-Catalyzed Conversion of 18:0-ACP to 18:1-ACP Measured at Varying Concentrations of Fd

Δ9D isoform	k_{cat} (min^{-1})[a]	K_M (mM)	k_{cat}/K_M ($mM^{-1}\,min^{-1}$)	R[b]
wild-type	28 (1.8)	0.56 (0.11)	50 (7.6)	0.981
K41A	30 (1.4)	0.54 (0.082)	55 (6.5)	0.986
K56A	42 (1.6)	18 (1.7)	2.4 (0.15)	0.992
K60A	40 (0.95)	3.2 (0.27)	12 (0.84)	0.997
K56A/K60A	30 (4)	140 (30)	0.2(0.02)	0.979
K230A	24 (3.8)	1,194 (327)	0.02 (0.006)	0.988
K56A/K60A/K230A[c]	ND[d]	ND	0.00007 (0.00008)	0.957

[a] The k_{cat} and K_M values were obtained from nonlinear least-squares fitting to eq 1. The k_{cat} values are reported per diiron center of Δ9D. [b] Correlation coefficient of the nonlinear least-squares fitting. [c] The product formation data were analyzed by linear least-squares fitting as described in Materials and Methods using the first-order assumption $d[18:1\text{-ACP}]/dt = v_o$ [Fd]. [d] Not determined.

constructed. This isoform retained the catalytic diiron centers as judged by iron analysis and optical spectroscopy, yet catalytic activity was nearly eliminated, even at Fd concentrations up to 2 mM (solid squares in Figure 4B). Under the assumption of low affinity for Fd, the detected rate of product formation corresponded to the first-order rate k_{cat}/K_M in the accessible concentration range for Fd. Table 2 shows that K56A/K60A/K230A Δ9D has a catalytic efficiency decreased by at least 700 000-fold relative to that of Δ9D.

Cross-Linking Reactions of Mutated Δ9D. The large increases in the apparent K_M values observed for K230A Δ9D and the doubly and triply mutated variants suggested that weaker binding affinities might also correspond to the decreased efficiency of the EDC and NHS reactions. Surprisingly, however, similar yields of the ~45 kDa product assigned to the cross-linking of Fd and Δ9D were observed in all reactions including complexes of Fd and K56A/K60A/K230A Δ9D, where the apparent affinity for Fd should have decreased by greater than 10^4, according to steady-state kinetic analysis.

Figure 5 and Table 3 summarize the results of the cross-linking of Fd and Δ9D in the presence of 18:0-ACP and resolve this apparent inconsistency. Figure 5 shows an SDS−PAGE analysis of cross-linking reactions between EDC-activated Fd and the preformed complexes of either Δ9D (Figure 5, P2 = Δ9D) or K56A/K60A Δ9D (Figure 5, P2 = K56A/K60A Δ9D, abbreviated as Δ9D* in the Figure) with 18:0-ACP (Figure 5, S) and other control reactions. Table 3 summarizes the results from comparable cross-linking reactions performed with the various mutated forms of Δ9D. Under the conditions used in these experiments, Δ9D was fully saturated with 18:0-ACP (K_{D1} = 13 nM, K_{D2} = 170 nM (*31*)). Lane 4 is a control that shows Δ9D and 18:0-ACP are separated by denaturing electrophoresis. This lane also shows that 18:0-ACP (an apparent mass of ~12 kDa) is partially converted into the holo-ACP dimer (an apparent mass of ~20 kDa) during electrophoresis. Moreover, lane 5 is a control that shows that EDC-activated Fd does not cross-link with 18:0-ACP.

Lanes 2 and 3 in Figure 5 show that EDC-activated Fd can be cross-linked to Δ9D to give the ~45 kDa complex in both the absence (lane 2) and presence of 18:0-ACP (lane 3). This result confirms that the binding of 18:0-ACP and Fd are not mutually exclusive. Thus, a ternary complex is a feasible intermediate in Δ9D catalysis.

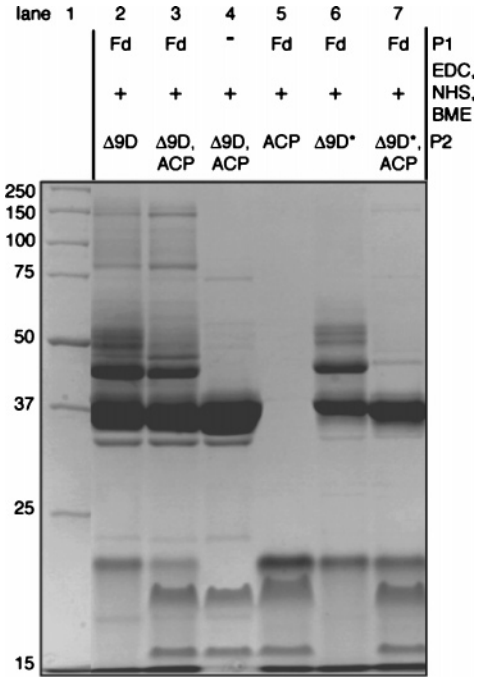

FIGURE 5: Coomassie-stained denaturing electrophoresis gel showing the influence of 18:0-ACP (abbreviated as ACP to fit the figure) on the cross-linking of Fd to either wt Δ9D (P2 = Δ9D) or K56A/K60A Δ9D (P2 = K56A/K60A Δ9D, abbreviated as Δ9D* to fit in the figure). Lane 1 contains molecular mass standards. The cross-linking of wt Δ9D in the absence (lane 2) or the presence (lane 3) of 18:0-ACP appears to be similar. Lane 4 shows Δ9D and 18:0-ACP in the presence of EDC, NHS, and BME. The cross-linking of K56A/K60A Δ9D is affected by the presence of 18:0-ACP (compare lanes 6 and 7). Activated Fd does not react with 18:0-ACP (lane 5). 18:0-ACP (~16 kDa) is partially converted to holo-ACP (~20 kDa) during electrophoresis.

Table 3: Results of Cross-Linking EDC-Activated Fd to Complexes of Δ9D Isoforms with 18:0-ACP

Δ9D isoform[a]	18:0-ACP[a]	cross-linking with EDC-Fd observed[b]
wt	−	+
K56A	−	+
K60A	−	+
K230A	−	+
K56A/K60A	−	+
K56A/K60A/K230A	−	+
wt	+	+
K56A	+	+
K60A	+	+
K230A	+	+
K56A/K60A	+	−
K56A/K60A/K230A	+	−

[a] Isoforms complexed with 18:0-ACP as indicated and then mixed with EDC-activated Fd as described in Materials and Methods. [b] Cross-linking products detected using SDS−PAGE as shown in Figure 5, lanes 6 and 7 for reactions containing K56A/K60A Δ9D with and without 18:0-ACP.

Lane 6 of Figure 5 shows that EDC-activated Fd can also be efficiently cross-linked to K56A/K60A Δ9D in the absence of 18:0-ACP, even as the K_M value of this Δ9D isoform was increased by ~250-fold (Table 2). Moreover, Table 3 indicates that EDC-activated Fd was also efficiently cross-linked to the triply mutated Δ9D. These results reveal the presence of an alternative Fd binding site on Δ9D after the proposed Fd binding site was eliminated by mutagenesis.

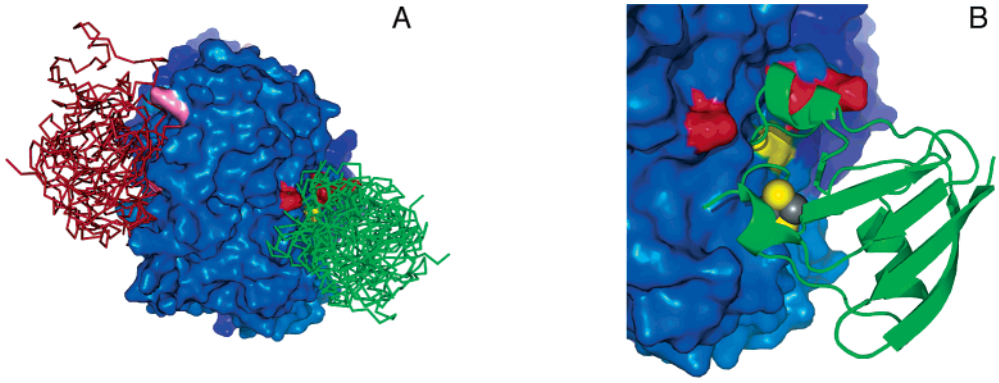

FIGURE 6: Predicted sites for protein−protein complex formation between Δ9D and Fd. This orientation allows a view of only one subunit of the Δ9D dimer. (A) Surface representation of Δ9D showing the lysine residues important in Fd binding (red), W62 (yellow), and lysine residues in the ACP binding site (violet). The Fd molecules docked at the proposed electron-transfer site are shown in green backbone trace, and the Fd molecules docked in the ACP binding site are shown in red backbone trace. (B) Close-up view of a representative Δ9D−Fd conformation with the coloring of the residues the same as that in A. In this conformation, the [2Fe-2S] cluster of Fd is ~11 Å away from W62.

Indeed, Table 3 shows that cross-linking was obtained among all combinations of the mutated Δ9D and Fd in the absence of 18:0-ACP.

Lane 7 of Figure 5 along with Table 3 shows that the cross-linking of Fd to either K56A/K60A Δ9D or K56A/K60A/K230A Δ9D was eliminated in the presence of 18:0-ACP. Because mutations of both K56 and K60 were required to prevent the cross-linking in the presence of 18:0-ACP, these two residues may have a distinct role in complex formation relative to the contributions of K230. The elimination of the cross-linking between Fd and the doubly and triply mutated Δ9D in the presence of 18:0-ACP is also notable in that it defines an overall specificity for protein−protein interactions because no alternative lysine residues on the surface of Δ9D were capable of yielding cross-linking with Fd. Therefore, we conclude that Fd has one functionally relevant binding site on the Δ9D surface close to K56 and K60 and that Fd can adventitiously cross-link to the 18:0-ACP binding site in the mutated Δ9D or in the absence of 18:0-ACP.

Docking Results. ClusPro (*27*, *28*) was used to investigate complexes of Fd (pdb file 1FXA) as the moving molecule and with Δ9D (pdb file 1AFR) as the static molecule. Figure 6A shows the locations of two favored regions for Fd binding on the Δ9D surface. From a total of 60 different conformations examined in detail, 17 were located close to our proposed Fd binding site, including K56, K60, K230 (red surface), and W62 (yellow surface). The green backbone traces represent an ensemble of six of these conformations at the Fd binding site of one subunit of Δ9D. Multiple conformations of Fd were also located close to the opening of the proposed 18:0-ACP binding channel, including the three closely spaced lysine residues K261, K262, and K322 (violet surface). The red backbone traces represent an ensemble of six Fds adventitiously bound at the 18:0-ACP binding site. The other Fd conformations examined were singletons, whose positions were distributed nearly all over the surface of Δ9D. It is notable, however, that none of these latter conformations contained Fds interacting with the surface of Δ9D closest to K41, which is likely due to steric factors. Thus, the docking experiments also support the conclusion that two different binding sites for Fd exist on the surface of Δ9D, with one binding site directed toward a catalytically relevant electron-transfer site and the other apparently overlapping with the high-affinity binding site for 18:0-ACP.

The set of 17 conformations at the proposed Fd binding site had individual conformations that placed the [2Fe-2S] cluster either close to or far from the surface of Δ9D. For the entire set of 17, the average distance from C41-SG (ligand of the [2Fe-2S] cluster of Fd) to W62-N of Δ9D was ~20 ± 10 Å. However, by selecting the seven binding conformations that had the [2Fe-2S] cluster oriented toward the Δ9D surface, the average distance shortened to 14 ± 4 Å. This distance compares favorably with the proposed optimal electron tunneling distance between two redox cofactors of ~14 Å (*32*). Figure 6B shows one representative conformation from this subset of Fd−Δ9D conformations.

A ClusPro docking of 18:0-ACP to Δ9D was also undertaken. From a total of 20 configurations examined, 18 clustered at the 18:0-ACP binding site defined here by the possible electrostatic contributions of K262, K262, and K322. Surprisingly, the 18:0-ACP configurations did not cluster at the proposed Fd binding site, which again may be due to steric considerations. Figure 7A shows one of the representative conformations for 18:0-ACP binding along with Fd bound at its proposed functional site to make a ternary complex with Δ9D. The ACP binding conformation places Ser36 (the position of covalent attachment of phosphopantetheine and acyl chain) close to the entry to the substrate channel leading to the diiron active site.

DISCUSSION

Electron-Transfer Pathways in Δ9D and Related Enzymes. An examination of the 3D structure showed that Fd has 21 carboxylate groups, including many on the surface close to the [2Fe-2S] cluster. Likewise, each subunit of Δ9D has 24 lysine residues. In combination, this number of functional groups suggests that many interactions might be potentially subjected to chemical cross-linking and belies the utility of cross-linking alone to reveal the molecular details of protein−protein interactions.

The crystal structure of Δ9D (*30*) revealed two possible pathways for electron transfer extending from the surface of the protein to the diiron center (Figure 1). One pathway includes amino acids W62, D228, and H146 and extends

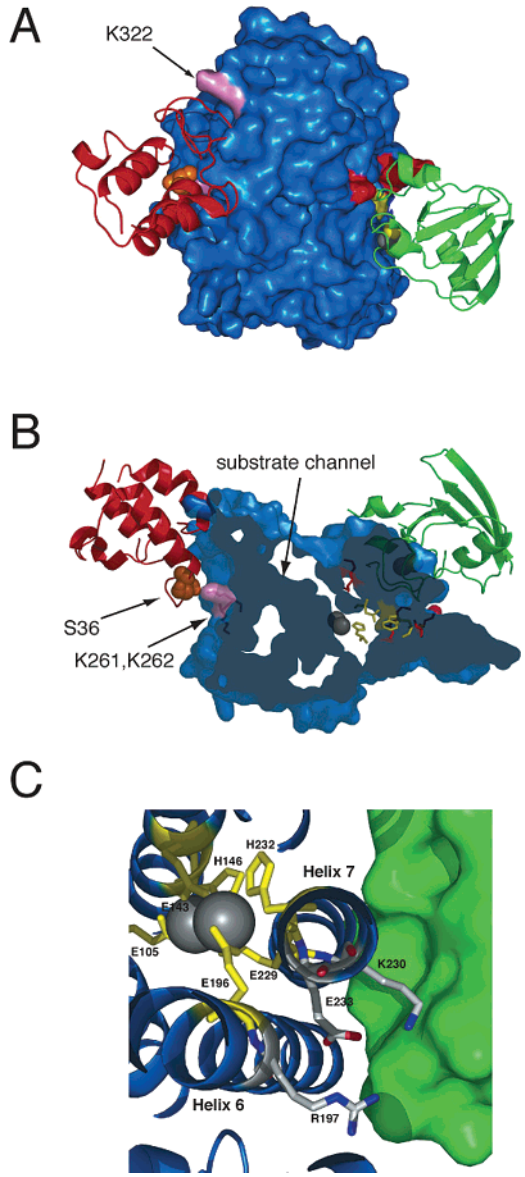

FIGURE 7: Model for the tertiary complex of Δ9D. This orientation allows a view of only one subunit of the Δ9D dimer. The Fd and ACP binding sites are separated by ~50 Å across the subunits of the Δ9D dimer. (A) Surface representation of Δ9D with Fd (green) and ACP (red) shown in ribbon representation. The lysine residues involved in forming the Fd binding site are shown in red, W62, D228, and H146 are shown in yellow, and the lysine residues in the ACP binding site are shown in pink. The S36 residue of ACP (the site of phosphopantetheinylation and acylation) is represented by orange spheres. (B) Clipped-view representation of Δ9D, revealing the position of the channel leading to the active-site diiron center (gray spheres). The Fd and ACP are in the same binding sites as those show in A. (C) Close-up view of the region of Δ9D near K230 in the model for the complex of Fd and Δ9D. K230 and E233 are found on the solvent-exposed face of helix 7, which also provides diiron ligands E229 and H232. E233 is hydrogen bonded to both K230 and R197. It is proposed that these interactions may be perturbed by Fd binding and thus alter the active site to facilitate catalysis.

from W62 at the surface loop region between helix-1 and helix-2 to internal diiron ligand H146 (Figure 1). Both *Escherichia coli* ribonucleotide reductase (*22*) and putative acyl-ACP desaturase DesA2 from *Mycobacterium tuberculosis (23)* have this triad of structurally homologous residues, but methane monooxygenase has R146 in this position as a substitute for W62 (*33*). In the *E. coli* enzyme, W48 is hydrogen-bonded to D237, which is hydrogen-bonded to diiron ligand H118. W48 forms a cation radical during tyrosyl radical formation, and the mutagenesis of W48 profoundly changes the outcome of single-turnover catalysis (*34*−*36*). Δ9D also has K230 in close proximity to K56 and K60. These three lysine residues are located 7.5, 14, and 7.3 Å, respectively, from W62. The combination of results presented here strongly implicates a role for these surface residues in Δ9D catalysis.

The Δ9D structure also showed that K41, the other surface lysine investigated in this work, is in close proximity to a proposed electron-transfer pathway (*30*) including amino acids W132, W135, W139, F189, and Y236 (Figure 1). These residues are completely buried and extend along the interior of the four-helix bundle toward diiron center ligand E143. These residues are mostly conserved in *M. tuberculosis* DesA2 (where the closest structurally comparable residues are W96, W99, W103, L152, and F196 respectively), less so in ribonucleotide reductase (F18, W107, W111, L197, and T245), and completely diverged in methane monooxygenase (M53 or Q133, Y137, Q140, T253 and Q205, and G250). Furthermore, the lack of effects upon mutation of K41 (Table 2) suggests that the proposed electron path involving W132 is not used in Δ9D catalysis.

Cross-Linking Implicates Carboxylate Residues from Fd and Lysine Residues from Δ9D. EDC-catalyzed cross-linking with SDS analysis showed that a distinct product with an apparent mass of ~45 kDa was formed only in reactions containing EDC-activated Fd and Δ9D (Figure 3, lane 9). An analysis by MALDI-MS confirmed that this cross-linked product consisted of Fd and a single subunit of dimeric Δ9D (Table 1). The reaction conditions (Figure 2) established that the covalent cross-link was generated between carboxylate groups from Fd and lysine(s) from Δ9D.

Catalytic Consequences of Lysine Mutations. The K41A mutation gave no change in either k_{cat} or k_{cat}/K_M values as compared to those for wt Δ9D. Therefore, no other lysine residues were studied in this region of Δ9D. In contrast, the apparent K_M values of the K56A, K60A, and K230A isoforms for Fd binding were substantially altered (Table 2), even as the k_{cat} values were not significantly changed as compared to those for wt Δ9D. Notably, the doubly mutated K60A/K56A Δ9D had an ~250-fold reduction in the apparent K_M value but no significant reduction in the k_{cat} value. Furthermore, the single mutation K230 caused an ~2200-fold reduction in the k_{cat}/K_M value, which was also primarily associated with a decrease in the apparent K_M value for Fd. The substitution of all three lysine residues effectively abolished the ability of wt Δ9D to recognize Fd as an electron partner (Table 2), although because of the sensitivity of the assay to 18:1 production, the triply mutated protein did indeed retain detectable ability to catalyze double-bond insertion. These results strongly implicate K56, K60, and K230 in one or more aspects of Δ9D catalysis but also suggest that these surface residues are not essential for the chemical steps of catalysis.

Effect of 18:0-ACP on Fd Cross-Linking. Cross-linking reactions undertaken using the catalytically relevant ternary complex of Δ9D, Fd, and 18:0-ACP (*16*) suggest that Fd can adventitiously cross-link to the 18:0-ACP binding site of the K56A/K60A- and K56A/K60A/K230A-mutated Δ9D in the absence of 18:0-ACP. In contrast, the cross-linking

of Fd to the doubly and triply mutated Δ9D was eliminated in the presence of 18:0-ACP (which likely blocks access to K261, K262, and K322), showing that no other lysine groups from Δ9D are involved in complex formation. Because ACP and Fd are small acidic proteins (~9 kDa with pI 3.8 and ~11 kDa with pI 3.9, respectively), it is reasonable that both may interact with Δ9D by carboxylate−lysine charge pairs. The originally proposed ACP binding region consists of a depression close to the opening of an extended channel leading to the diiron center (*30*). This depression is on the opposite side of the Δ9D monomer from the proposed Fd binding site encompassing K56, K60, W62, and K230 (Figures 6A and 7A and B). Because 18:0-ACP exhibits nanomolar binding affinities (*31*), its presence would likely eliminate adventitious Fd binding, which is apparently several orders of magnitude weaker (Table 2) (*31*).

Further consideration of the results of Figure 5 and Table 3 reveals that K56 and K60 are essential for the formation of a cross-linked complex between Fd and Δ9D, supporting a role for these lysine residues in the formation of an electrostatic complex at the proposed electron-transfer site during catalysis. Because the presence of K230 in the doubly mutated Δ9D did not lead to the formation of the diagnostic ~45 kDa cross-linked adduct (Table 3), the strong contribution of this lysine residue to catalysis (Table 2) may arise from a different role than electrostatic complex formation.

Other Studies of Fd−Protein Interactions. EDC-catalyzed cross-linking of the [2Fe-2S] Fd domain of the reductase and hydroxylase components of methane monooxygenase yielded a cross-link between the acidic residues from the Fd domain (E56 and E91) and the *N*-terminus of the hydroxylase (*37*). The Fd domain has 19 carboxylate residues, whereas the hydroxylase has 122 lysine residues. Whether the Fd domain has the same binding interactions as the intact reductase has not been determined. However, in a related study (*38*), no significant line broadening of the ^{1}H ^{15}N HSQC cross peaks assigned to Fd domain residues E56 and E91 occurred upon addition of the hydroxylase.

Ferredoxins from several other enzyme complexes have been cross-linked to their physiological redox partners through acidic residues (*39*, *40*). For example, an acidic residue from Fd has been shown to cross-link to Fd:$NADP^+$ reductase (*41*) and to photosystem I in reactions containing EDC (*39*). The binding interactions and the electron-transfer reaction between Fd and Fd:$NADP^+$ reductase from *Anabaena* have been studied extensively (*42*−*45*), and these results show that electrostatic interactions are largely mediated by acidic residues from Fd (*46*) and basic residues from Fd:$NADP^+$ reductase. These interactions are important for steering the two proteins into the correct orientation for electron transfer (*47*). In the crystal structure of the Fd-Fd:$NADP^+$ complex (*45*), a salt bridge between E94 from Fd and K75 from Fd:$NADP^+$ reductase was observed at the protein−protein interface. Site-directed mutagenesis of K75 from Fd:$NADP^+$ reductase increased the K_M value for Fd binding by at least 50-fold, whereas no effect was observed on the k_{cat} value (*43*), suggesting an electrostatic role for K75 in the formation of the Fd−Fd:$NADP^+$ complex. A similar magnitude of increase in the K_M value for Fd binding and no change in the k_{cat} value was observed with the K60A mutation of Δ9D, further supporting the role of this lysine residue in electrostatic contributions to the orientation of Fd binding.

Δ9D Tertiary Complex. It is reasonable to assume that a functional Fd binding site on Δ9D will place the [2Fe-2S] cluster and diiron cofactor in close proximity to facilitate electron transfer during multiple turnover catalysis. Whereas two of the cysteine ligands to the [2Fe-2S] cluster in Fd are solvent exposed (*29*), all of the ligands to the diiron center of Δ9D are buried within a four-helix bundle (*30*). Thus, electron transfer from Fd to the diiron center of Δ9D is presumably facilitated by the alignment of the two protein surfaces through amino acid contacts. Our results also indicate that 18:0-ACP binding precedes electron transfer (*16*). Indeed, many of the models calculated for the docking of 18:0-ACP with Δ9D predict the interactions of ACP with K261, K262, and K322. These lysine residues are on the opposite face of the Δ9D subunit from the lysines proposed to interact with Fd in the electron-transfer reactions (~38 Å apart). Furthermore, the proposed 18:0-ACP and Fd binding sites are separated by ~50 Å between subunits and, therefore, are unlikely to spatially overlap. Figure 7A provides a model for the ternary complex of Fd and 18:0-ACP with one subunit of the Δ9D dimer.

Figure 7B shows a more detailed view of the docked position of ACP and the extent of the substrate-binding channel. This channel proceeds from the surface toward the diiron center and the region of helix-7 containing K230 and E233. It has been previously demonstrated that 18:0-ACP binding causes structural changes in the active site of sodium dithionite-reduced Δ9D. However, these changes were not sufficient to permit O_2-dependent desaturation but instead led to the formation of a quasi-stable unreactive peroxo intermediate (*14*, *15*). One possibility accounting for the lack of reactivity of the sodium dithionite-reduced Δ9D might be that Fd binding is required to promote further reactivity. Thus the occupation of the substrate channel by an 18:0 acyl chain could lead to conformation changes that optimize the Fd binding site for efficient electron transfer, promotion of ligand rearrangements that lead to O_2 activation (*12*), or other aspects. Alternatively, Fd binding may transmit information into the active site that optimally aligns the acyl chain to allow catalysis to proceed.

Recent X-ray studies of methane monooxygenase revealed conformational changes in helix E in the presence of a relatively large alternative product, 6-bromohexan-1-ol (*48*). Similar conformational changes may occur upon the formation of the more extensive interactions predicted by the binding of 18:0-ACP with Δ9D (Figure 7B). Upon formation of the 18:0-ACP and Δ9D complex, it is also feasible that any rearrangements caused by binding could be transmitted to the region of helix 7 including K230. Figure 7C shows that K230 is within hydrogen-bonding distance of E233, the latter of which also forms an ion pair with R197. R197 is located in helix 6, which is structurally homologous to helix E of methane monooxygenase. K230 and E233 are adjacent to diiron ligands E229 and H232, whereas R197 is adjacent to diiron ligand E196. By making contacts with K230, the binding of Fd may alter this configuration of residues situated close to or in the active site.

Implications for the Δ9D Mechanism. These studies have provided new insight into the protein−protein interactions required for Δ9D catalysis. Our proposed location of the Fd

binding site has been supported by biochemical, catalytic, and computational approaches. This preferred binding site involves surface complementarity and electrostatic interactions between Fd and Δ9D. The site also appears to encompass a set of surface residues from Δ9D that may lead to conformational changes from the binding of either 18:0-ACP or Fd. The presence of only one Fd binding site implies that two molecules of Fd must successively bind at this position to provide the $2e^-$ required for catalysis. The exact nature and timing of molecular events encompassed by the reaction cycle are presently not known, but a number of intriguing possibilities can be considered in light of this model.

ACKNOWLEDGMENT

We thank Dr. Julie Mitchell (University of Wisconsin) for helpful discussions on modeling the Δ9D−Fd complex.

REFERENCES

1. Fox, B. G., Shanklin, J., Somerville, C., and Münck, E. (1993) Stearoyl-acyl carrier protein Δ^9 desaturase from *Ricinus communis* is a diiron-oxo protein, *Proc. Natl. Acad. Sci. U.S.A. 90*, 2486-2490.
2. Shanklin, J., and Cahoon, E. B. (1998) Desaturation and related modifications of fatty acids, *Annu. Rev. Plant Physiol. Plant Mol. Biol. 49*, 611−641.
3. Nordlund, P., and Eklund, H. (1995) Di-iron-carboxylate proteins, *Curr. Opin. Struct. Biol. 5*, 758−766.
4. Leahy, J. G., Batchelor, P. J., and Morcomb, S. M. (2003) Evolution of the soluble diiron monooxygenases, *FEMS Microbiol. Rev. 27*, 449−479.
5. Wallar, B. J., and Lipscomb, J. D. (1996) Dioxygen activation by enzymes containing binuclear non-heme iron clusters, *Chem. Rev. 96*, 2625−2657.
6. Fox, B. G. (1997) in *Comprehensive Biological Catalysis* (Sinnott, M., Ed.) pp 261−348, Academic Press, London.
7. Merkx, M., Kopp, D. A., Sazinsky, M. H., Blazyk, J. L., Muller, J., and Lippard, S. J. (2001) Dioxygen activation and methane hydroxylation by soluble methane monooxygenase: A tale of two irons and three proteins, *Angew. Chem., Int. Ed. 40*, 2782−2807.
8. Thiel, E. C. (2005) Ferritin: dynamic management of biological iron and oxygen chemistry, *Acc. Chem. Res. 38*, 167−175.
9. deMare, F., Kurtz, D. M., Jr., and Nordlund, P. (1996) The structure of *Desulfovibrio vulgaris* rubrerythrin reveals a unique combination of rubredoxin-like FeS4 and ferritin-like diiron domains, *Nat. Struct. Biol. 3*, 539−546.
10. Haas, J. A., and Fox, B. G. (1999) Role of hydrophobic partitioning in substrate selectivity and turnover of the *Ricinus communis* stearoyl acyl carrier portein Δ^9 desaturase, *Biochemistry 38*, 12833−12840.
11. McKeon, T. A., and Stumpf, P. K. (1982) Purfication and characterization of the stearoyl-acyl carrier protein desaturase and the acyl-acyl carrier protein thioesterase from maturing seeds of safflower, *J. Biol. Chem. 257*, 12141−12147.
12. Yang, Y., Broadwater, J. A., Pulver, S. C., Fox, B. G., and Solomon, E. I. (1999) Circular dichroism and magnetic circular dichroism studies of the reduced binuclear non-heme iron site of stearoyl-ACP Δ^9 desaturase: Substrate binding and comparison to ribonucleotide reductase, *J. Am. Chem. Soc. 121*, 2770−2783.
13. Skulan, A. J., Brunold, T. C., Baldwin, J., Saleh, L., Bollinger, J. M., Jr., Solomon, E. I (2004) Nature of the peroxo intermediate of the W48F/D84E ribonucleotide reductase variant: Implications for O_2 activation by binuclear non-heme iron enzymes, *J. Am. Chem. Soc. 126*, 8842−8855.
14. Broadwater, J. A., Ai, J., Loehr, T. M., Sanders-Loehr, J., and Fox, B. G. (1998) Peroxodiferric intermediate of stearoyl-acyl carrier protein Δ^9 desaturase: Oxidase reactivity during single turnover and implications for the mechanism of desaturation, *Biochemistry 37*, 14664−14671.
15. Broadwater, J. A., Achim, C., Münck, E., and Fox, B. G. (1999) Mössbauer studies of the formation and reactivity of a quasi-stable peroxo intermediate of stearoyl-acyl carrier protein Δ^9-desaturase, *Biochemistry 38*, 12197−12204.
16. Lyle, K. S., Haas, J. A., and Fox, B. G. (2003) Rapid-mix and chemical quench studies of ferredoxin-reduced stearoyl-acyl carrier protein desaturase, *Biochemistry 42*, 5857−5866.
17. Fox, B. G., Froland, W. A., Dege, J. E., and Lipscomb, J. D. (1989) Methane monooxygenase from *Methylosinus trichosporium* OB3b purification and properties of a three-component system with high specific activity from a type II methanotroph, *J. Biol. Chem. 264*, 10023−10033.
18. Froland, W. A., Andersson, K. K., Lee, S.-K., Liu, K., and Lipscomb, J. D. (1992) Methane monooxygnease component B and reductase alter the regioselectivity of the hydroxylase component-catalyzed reactions: A novel role for protein-protein interactions in an oxygenase mechanism, *J. Biol. Chem. 267*, 17588−17597.
19. Lee, S.-K., Nesheim, J. C., and Lipscomb, J. D. (1993) Transient intermediates of the methane monooxygenase catalytic cycle, *J. Biol. Chem. 268*, 21569−21577.
20. Valentine, A. M., Stahl, S. S., and Lippard, S. J. (1999) Mechanistic studies of the reaction of reduced methane monooxygenase hydroxylase with dioxygen and substrates, *J. Am. Chem. Soc. 121*, 3876−3887.
21. Lynch, J. B., Juarez-Garcia, C., Münck, E., and Que, L. J. (1989) Mössbauer and EPR studies of the binuclear iron center in ribonucleotide reductase from *Escherichia coli*, *J. Biol. Chem. 264*, 8091−8096.
22. Nordlund, P., and Eklund, H. (1993) Structure and function of the *Escherichia coli* ribonucleotide reductase protein R2, *J. Mol. Biol. 232*, 123−164.
23. Dyer, D. H., Lyle, K. S., Rayment, I., and Fox, B. G. (2005) X-ray structure of putative acyl-ACP desaturase DesA2 from *Mycobacterium tuberculosis* H37Rv, *Protein Sci. 14*, 1508−17.
24. Cheng, H., Westler, W. M., Xia, B., Oh, B., and Markley, J. L. (1995) Protein expression, selective isotopic labeling, and analysis of hyperfine-shifted NMR signals of *Anabaena* 7120 vegetative [2Fe-2S] ferredoxin, *Arch. Biochem. Biophys. 316*, 619−634.
25. Sehgal, D., and Vijay, I. K. (1994) A method for the high efficiency of water-soluble carbodiimide-mediated amidation, *Anal. Biochem. 218*, 87−91.
26. Hoffman, B. J., Broadwater, J. A., Johnson, P., Harper, J., Fox, B. G., and Kenealy, W. R. (1995) Lactose fed-batch overexpression of recombinant metalloproteins in *Escherichia coli* BL21-(DE3): Process control yielding high levels of metal-incorporated, soluble protein, *Protein Expression Purif. 6*, 646−654.
27. Comeau, S. R., Gatchell, D. W., Vajda, S., and Camacho, C. J. (2004) ClusPro: A fully automated algorithm for protein-protein docking, *Nucleic Acids Res. 32*, W96−99.
28. Comeau, S. R., Gatchell, D. W., Vajda, S., and Camacho, C. J. (2004) ClusPro: An automated docking and discrimination method for the prediction of protein complexes, *Bioinformatics 20*, 45−50.
29. Rypniewski, W. R., Breiter, D. R., Benning, M. M., Wesenberg, G., Oh, B.-H., Markley, J. L., Rayment, I., Holden, H. M. (1991) Crystallization and structure determination to 2.5-Å resolution of the oxidized [2Fe-2S] ferredoxin isolated from *Anabaena* 7120, *Biochemistry 30*, 4126−4131.
30. Lindqvist, Y., Huang, W., Schneider, G., and Shanklin, J. (1996) Crystal structure of stearoyl-acyl carrier protein Δ^9 desaturase from castor seed and its relationship to other diiron proteins, *EMBO J. 15*, 4081−4092.
31. Haas, J. A., and Fox, B. G. (2002) Fluorescence anisotropy studies of enzyme−substrate complex formation in stearoyl-ACP desaturase, *Biochemistry 41*, 14472−14481.
32. Page, C. C., Moser, C. C., Chen, X., and Dutton, L. P. (1999) Natural engineering principles of electron tunnelling in biological oxidation-reduction, *Nature 402*, 47−52.
33. Rosenzweig, A. C., Frederick, C. A., Lippard, S. J., and Nordlund, P. (1993) Crystal structure of a bacterial nonhaem iron hydroxylase that catalyses the biological oxidation of methane, *Nature 366*, 537−43.
34. Baldwin, J., Krebs, K., Ley, B. A., Edmondson, D. E., Huynh, B. H., and Bollinger, J. M. (2000) Mechanism of rapid electron transfer during oxygen activation in the R2 subunit of *Escherichia coli* ribonucleotide reductase. 1. Evidence for a transient tryptophan radical, *J. Am. Chem. Soc. 122*, 12195−12206.
35. Krebs, C., Chen, S., Baldwin, J., Ley, B. A., Patel, U., Edmondson, D. E., Huynh, B. H., and Bollinger, J. M., Jr. (2000) Mechanism of rapid electron transfer during oxygen activation in the R2 subunit of *Escherichia coli* ribonucleotide reductase. 2. Evidence

for and consequences of blocked electron transfer in the W48F variant, *J. Am. Chem. Soc. 122*, 12207−12219.
36. Bollinger, J. M., Jr., Tong, W. H., Ravi, N., Huynh, B. H., Edmondson, D. E., and Stubbe, J. (1994) Mechanism of assembly of the tyrosyl radical-diiron(III) cofactor of *E. coli* ribonucleotide reductase. 3. Kinetics of the limiting Fe^{2+} reaction by optical, EPR, and Möessbauer spectroscopies, *J. Am. Chem. Soc. 116*, 8024−8032.
37. Kopp, D. A., Berg, E. A., Costello, C. E., and Lippard, S. J. (2003) Structural features of covalently cross-linked hydroxylase and reductase proteins of soluble methane monooxygenase as revealed by mass spectrometric analysis, *J. Biol. Chem. 278*, 20939−20945.
38. Muller, J., Lugovskoy, A. A., Wagner, G., and Lippard, S. J. (2002) NMR structure of the [2Fe-2S] ferredoxin domain from soluble methane monooxygenase reductase and interaction with its hydroxylase, *Biochemistry 41*, 42−51.
39. Lelong, C., Setif. P., Lagoutte, B., and Bottin, H. (1994) Identification of the amino acids involved in the functional interaction between photosystem I and ferredoxin from *Synechocystis* sp. PCC 6803 by chemical cross-linking, *J. Biol. Chem. 269*, 10034−10039.
40. Golinelli, M. P., Gagnon, J., and Meyer, J. (1997) Specific interaction of the [2Fe-2S] ferredoxin from *Clostridium pasteurianum* with the nitrogenase MoFe protein, *Biochemistry 36*, 11797−11803.
41. Zanetti, G., Morelli, D., Ronchi, S., Negri, A., Aliverti, A., and Curti, B. (1988) Structural studies on the interaction between ferredoxin and ferredoxin-$NADP^+$ reductase, *Biochemistry 27*, 3753−3759.
42. Nogues, I., Martinez-Julvez, M., Navarro, J. A., Hervas, M., Armenteros, L., Angel de la Rosa, M., Brodie, T. B., Hurley, J. K., Tollin, G., Gomez-Moreno, C., and Medina, M. (2003) Role of hydrophobic interactions in the flavodoxin mediated electron transfer from photosystem I to ferredoxin-$NADP^+$ reductase in *Anabaena* PCC 7119, *Biochemistry 42*, 2036−2045.
43. Martinez-Julvez, M., Medina, M., Hurley, J. K., Hafezi, R., Brodie, T. B., Tollin, G., and Gomez-Moreno, C. (1998) Lys75 of *Anabaena* ferredoxin-$NADP^+$ reductase is a critical residue for binding ferredoxin and flavodoxin during electron transfer, *Biochemistry 37*, 13604−13613.
44. Hurley, J. K., Weber-Main, A. M., Stankovich, M. T., Benning, M. M., Thoden, J. B., Vanhooke, J. L., Holden, H. M., Chae, Y. K., Xia, B., Cheng, H., Markley, J. L., Martinez-Julvez, M., Gomez-Moreno, C., Schmeits, J. L., and Tollin, G. (1997) Structure−function relationships in anabaena ferredoxin: Correlations between X-ray crystal structures, reduction potentials, and rate constants of electron transfer to ferredoxin:$NADP^+$ reductase for site-specific ferredoxin mutants, *Biochemistry 36*, 11100−11117.
45. Morales, R., Charon, M.-H., Kachalova, G., Serre, L., Medina, M., Gomez-Moreno, C., and Frey, M. (2000) A redox-dependent interaction between two electron-transfer partners involved in photosynthesis, *EMBO Rep. 1*, 271−276.
46. Hurley, J. K. M. R., Martinez-Julvez, M., Brodie, T. B., Medina, M., Gomez-Moreno, C., and Tollin, G. (2002) Structure-function relationships in anabaena ferredoxin/ferredoxin-$NADP^+$ reductase electron transfer: Insights from site-directed mutagenesis, transient absorption spectroscopy, and X-ray crystallography, *Biochim. Biophys. Acta 1554*, 5−21.
47. De Pascalis, A. R., Jelesarov, I., Ackermann, F., Koppenol, W. H., Hirasawa, M., Knaff, D. B., and Bosshard, H. R. (1993) Binding of ferredoxin to ferredoxin:$NADP^+$ reductase: The role of carboxyl groups, electrostatic surface potential, and molecular dipole moment, *Protein Sci. 2*, 1126−1135.
48. Sazinsky, M. H., and Lippard, S. J. (2005) Product bound structures of the soluble methane monooxygenase hydroxylase from *Methylococcus capsulatus* (bath): Protein motion in the alpha-subunit, *J. Am. Chem. Soc. 127*, 5814−5825.

BI0600547